

Effects of a magnetic field on vortex states in superfluid $^3\text{He-B}$

Kenichi Kasamatsu,¹ Ryota Mizuno,² Tetsuo Ohmi,¹ and Mikio Nakahara^{3,4}

¹*Department of Physics, Kindai University, Higashi-Osaka, Osaka 577-8502, Japan*

²*Department of Physics, Osaka University, 1-1 Machikaneyama-cho, Toyonaka, Osaka 560-0043, Japan*

³*Department of Mathematics, Shanghai University, 99 Shangda Road, Shanghai 200444, China*

⁴*Research Institute for Science and Technology, Kindai University, Higashi-Osaka 577-8502, Japan*



(Received 9 January 2019; published 18 March 2019)

Superfluid $^3\text{He-B}$ possesses three locally stable vortices known as a normal-core vortex (o vortex), an A -phase-core vortex (v vortex), and a double-core vortex (d vortex). In this work, we study the effects of a magnetic field ($\lesssim 0.1$ T) parallel or perpendicular to the vortex axis on these structures by solving the two-dimensional Ginzburg-Landau equation for two different sets of strong coupling correction. The energies of the v and d vortices have nontrivial dependence on the magnetic field. As the parallel magnetic field increases, the v vortex is energetically unstable even at high pressures and the d vortex becomes energetically most stable at all possible pressures. In perpendicular magnetic field, the energy of the v vortex is lower than that of the d vortex in the high pressure regime. In addition, the orientation of the double cores in the d vortex prefers to be parallel to the magnetic field at low pressures, while the d vortex with the double cores perpendicular to the magnetic field is allowed to continuously deform into the v vortex with increasing pressure.

DOI: [10.1103/PhysRevB.99.104513](https://doi.org/10.1103/PhysRevB.99.104513)

I. INTRODUCTION

Superfluid ^3He is a typical anisotropic fermionic superfluid consisting of spin-triplet p -wave Cooper pairs [1]. The order parameter of superfluid ^3He is characterized by 3×3 complex fields, which allows an existence of a rich variety of topological excitations. An example of topological excitations is a quantized vortex. Quantized vortices in superfluid ^3He involve extremely rich physical phenomena and this topic has been studied for decades [2,3].

Quantized vortices in superfluid ^3He are classified by the symmetry property [4,5]. Several types of axisymmetric vortices exist, depending on which discrete symmetries are preserved in the order parameter of the vortex states. The actual vortex structure at given temperature and pressure is obtained by minimizing the appropriate free energy.

For the $^3\text{He-B}$ phase, from many theoretical studies, it has been known that three types of vortices exist as the local minima of the free energy. One possible structure is known as the o vortex [6,7], which preserves the maximal symmetry group and its core is filled with the normal component. However, the o vortex is not the absolute energy minimum state in the parameter region where the B phase is stable [4,8]. Another axisymmetric vortex is the v vortex [4,8], which has magnetic reflection symmetry on a plane including the vortex line. The core of the v vortex is filled with the A -phase and the β -phase components. In experiments, the v vortex exists in high-temperature and high-pressure region in the p - T phase diagram of superfluid $^3\text{He-B}$ [9].

For low-temperature and low-pressure region, however, the axisymmetry of the v vortex is spontaneously broken into the double vortex-core structure, known as the d vortex. Thuneberg revealed this double-core structure by direct numerical minimization of the Ginzburg-Landau (GL) free

energy functional [10,11]. The d vortex can be interpreted as two half-quantum vortices bound together by the planar phase [10–12]. The nonaxisymmetric feature of the d vortex has been experimentally observed by Kondo *et al.* [13] through the measurement of a new Goldstone mode associated with the spiral twisting of the anisotropic core. The vortex core structure has been also calculated based on the quasiclassical Eilenberger equation [14–16]. This method is applicable to the weak-coupling regime, although it cannot explain the pressure dependence of the vortex structure in the strong-coupling regime.

The purpose of this paper is to analyze the influence of a magnetic field on the stability of the aforementioned vortices. We calculate the energy of the vortices using the GL free energy, and construct the phase diagram of vortices in the pressure and magnetic-field-strength plane. Here, the effect of a magnetic field is included through the quadratic term in the GL free energy. The energetic stability is nontrivial because the magnetic field suppresses some order parameter components in the core of the v and d vortices. To obtain the reliable results for the vortex energy, it is important to use the newly proposed values of the strong coupling correction for the β parameters in the bulk GL free energy [17]. To this end, we adapt two different data sets. One is the Sauls-Serene values (set I) [18], which was employed in the seminal paper by Thuneberg [10,11]. The other is obtained by optimizing various experimental data [19] (set II).

We find that, although both parameter sets give qualitatively similar vortex phase diagrams without a magnetic field, set II provides it closer to the experimental observations. When a magnetic field parallel to the vortex axis is turned on within the range where the bulk B phase is thermodynamically stable, the d vortex is the most stable structure throughout the pressure range. A magnetic field perpendicular to the vortex

axis stabilizes the v vortex; as the field strength increases, the stable region of the v vortex extends to the lower pressure region. It also breaks the rotational degeneracy with respect to the symmetry axis of the d vortex.

This paper is organized as follows. In Sec. II A, we outline the GL free energy required to analyze the vortex structure in superfluid ^3He - B and list two sets of parameters in the energy functional. Section II B briefly reviews the bulk energy of superfluid ^3He and Sec. II C describes the prescription of the numerical calculation. In Sec. II D, we show the numerical results for the case without the magnetic field, which is compared with those of the previous literature to confirm the validity of our calculation. Section III is the main part of our paper, where we show the numerical analysis of vortices in the presence of a magnetic field parallel (Sec. III A) and perpendicular (Sec. III B) to the vortex axis. Section IV is devoted to conclusion.

II. GINZBURG-LANDAU THEORY OF VORTEX STATES IN SUPERFLUID ^3He

We first introduce a formulation based on the GL free energy functional for the order parameter of superfluid ^3He . After describing the numerical procedure of the energy minimization, we analyze vortices in the B phase without a magnetic field and compare the results with those of the previous work to justify our calculation. We repeat the calculation with the parameters set I and set II for the strong coupling corrections and reproduce the results in Thuneberg [10, 11] for set I. The results for set II have not been reported before.

A. Ginzburg-Landau free energy

The order parameter of superfluid ^3He is given by a gap function $\hat{\Delta}$, which is a symmetric 2×2 matrix in spin space [1, 2]. By introducing the \mathbf{d} vector $\mathbf{d} = (d_x, d_y, d_z)$, the gap function can be written as $\hat{\Delta} = id_\mu \sigma_\mu \sigma_y$, where $\boldsymbol{\sigma} = (\sigma_x, \sigma_y, \sigma_z)$ is the Pauli matrix and summation over repeated indices is understood. By incorporating the representation $d_\mu = A_{\mu i} \hat{p}_i$ with unit vector $\hat{\mathbf{p}} = (\hat{p}_x, \hat{p}_y, \hat{p}_z)$ of the momentum on the Fermi surface, we write

$$\hat{\Delta}(\hat{\mathbf{p}}) = iA_{\mu i} \sigma_\mu \sigma_y \hat{p}_i, \quad (\mu, i = x, y, z). \quad (1)$$

Thus superfluid ^3He is characterized by complex tensor $(A_{\mu i})$ inherent in the p -wave ($L = 1$) and spin-triplet ($S = 1$) pairing, where μ and i refer to the spin and the orbital indices, respectively.

The GL theory is valid when we confine ourselves within the situation near the superfluid transition temperature $T \lesssim T_c$. By using $A_{\mu i}$, the bulk free energy density in the GL expansion takes the form

$$\begin{aligned} f_B = & -\alpha(t) A_{\mu i}^* A_{\mu i} + \beta_1 A_{\mu i}^* A_{\mu i}^* A_{\nu j} A_{\nu j} \\ & + \beta_2 A_{\mu i}^* A_{\mu i} A_{\nu j}^* A_{\nu j} + \beta_3 A_{\mu i}^* A_{\nu i}^* A_{\mu j} A_{\nu j} \\ & + \beta_4 A_{\mu i}^* A_{\nu i} A_{\nu j}^* A_{\mu j} + \beta_5 A_{\mu i}^* A_{\nu i} A_{\nu j} A_{\mu j}^*, \end{aligned} \quad (2)$$

which is invariant under separate spin and real space rotations in addition to the gauge transformation, namely $U(1) \times \text{SO}^{(S)}(3) \times \text{SO}^{(L)}(3)$. The coefficient $\alpha(t)$ of the second order term has a temperature dependence $\alpha(t) = \alpha_0 t$

TABLE I. List of the coefficients for the fitting of the correction of β according to the paper by Sauls and Serene [18]. Write ‘‘set I.’’

j	$A_j^{(1)}$	$A_j^{(2)}$	$A_j^{(3)}$	$A_j^{(4)}$
1	-0.041318	0.015586	-0.0043854	0.00044482
2	-0.13306	0.081867	-0.025704	0.0030876
3	-0.18713	0.10679	-0.030986	0.0037026
4	-0.28746	0.14638	-0.043984	0.0054785
5	-0.24049	0.090797	-0.023003	0.0015738

with a constant α_0 and a small parameter $t = 1 - T/T_c$. We consider the pressure range $0 \leq p \leq 3.44$ MPa, beyond which the system solidifies. The fourth order contribution to the bulk free energy has five terms with coefficients β_j . In the weak-coupling limit at zero pressure, these coefficients satisfy the relation

$$-2\beta_1^{\text{wc}} = \beta_2^{\text{wc}} = \beta_3^{\text{wc}} = \beta_4^{\text{wc}} = -\beta_5^{\text{wc}} \equiv 2\beta_0, \quad (3)$$

where $\beta_0 = 7\zeta(3)N(0)/[120\pi^2(k_B T_c)^2]$ with the density of states at the Fermi surface per spin $N(0)$ and the Riemann zeta function $\zeta(3)$. The pressure dependence can be included by the strong-coupling corrections for β_j , which are written as $\Delta\tilde{\beta}_j = \Delta\beta_j/\beta_0 = (\beta_j - \beta_j^{\text{wc}})/\beta_0$. However, the exact values of the correction as functions of the pressure are not known. Here, we use two data sets. One is the theoretical evaluation by Sauls and Serene [18]. In their paper, the values of $\Delta\tilde{\beta}_j$ for six values of pressure are given. In our work, these points and $\Delta\tilde{\beta}_j = 0$ at $p = 0$, where $\beta_j(p = 0)$ coincide with the weak-coupling values of Eq. (3), are interpolated through the fourth-order polynomials $\Delta\tilde{\beta}_j = \sum_{k=1}^4 A_j^{(k)} p^k$ as shown in Fig. 1(a), where p (MPa) is pressure. The list of the fitting parameters $A_j^{(k)}$ are shown in Table I. We refer to this set of β_j as ‘‘set I.’’

The other is described in Choi *et al.* [19], which reports a new data of the β_i values as functions of the pressure based on past experiments. The thermodynamic properties of superfluid ^3He have been better accounted for by the analysis with these new β_j values [20]. We also use the values of β_j following Ref. [19]; numerical fitting of the data with the ninth-order polynomials $\Delta\tilde{\beta}_j = \sum_{k=0}^9 B_j^{(k)} p^k$ is shown in Fig. 1(b), where the coefficients $B_j^{(k)}$ are listed in Table II. We refer to this set of β_j as ‘‘set II.’’ The obvious differences between Figs. 1(a) and 1(b) are that the values of β_i at $p = 0$ are slightly shifted from the weak-coupling values, and the magnitude of the correction is relatively large for β_3 and β_4 in Fig. 1(b); especially $\Delta\beta_5$ gives a positive correction in contrast with the set I case. This parameter set energetically favors the emergence of the A -phase component in the bulk phase diagram compared to the case of set I, as seen in Ref. [20] and discussed below.

The gradient energy in the GL expansion is given by

$$f_G = K_1 \partial_i A_{\mu j} \partial_i A_{\mu j}^* + K_2 \partial_i A_{\mu i} \partial_j A_{\mu j}^* + K_3 \partial_i A_{\mu j} \partial_j A_{\mu i}^*. \quad (4)$$

The coefficients K_i satisfy $K_1 = K_2 = K_3 = K$ in the weak-coupling limit, which we employ in the rest of this paper for simplicity. By comparing the gradient term and the first term

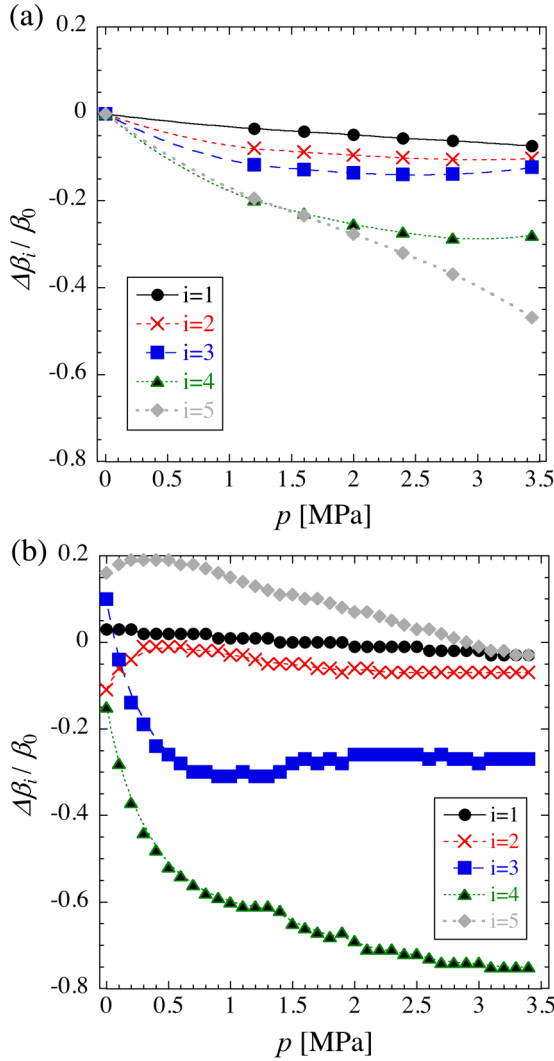


FIG. 1. Strong coupling correction $\Delta\beta_i$ ($i = 1-5$). The data points are taken from Ref. [18] (set I) (a) and Ref. [19] (set II) (b), and the curves represent the interpolating functions.

of the bulk energy [Eq. (2)], the coherence length is defined as

$$\xi(t) = \sqrt{\frac{K}{\alpha(t)}} = \sqrt{\frac{K}{\alpha_0}} \frac{1}{\sqrt{t}}. \quad (5)$$

The minimum length scale of our problem is the coherence length at zero temperature $\xi(0) = \sqrt{K/\alpha_0} \sim 0.01 \mu\text{m}$.

In this work, we consider the effect of a magnetic field on the vortex state. We take account of this effect through the

second order magnetic free energy given by

$$f_M = g_m H_\mu A_{\mu i}^* H_\nu A_{\nu i}, \quad (6)$$

where the coefficient g_m is given in the weak-coupling limit as

$$g_m^{\text{wc}} = \frac{7\zeta(3)N(0)(\gamma\hbar)^2}{48[(1+F_0^a)\pi k_B T_c]^2} \quad (7)$$

with the gyromagnetic ratio $\gamma = -2.04 \times 10^5 \text{ mT}^{-1} \text{ sec}^{-1}$ and the Landau parameter $F_0^a = -0.695$ at zero pressure. The pressure dependence of g_m was also reported in Ref. [19], where g_m is close to its weak-coupling value g_m^{wc} in $0 \leq p \leq 3.44 \text{ MPa}$. Thus we assume $g_m = g_m^{\text{wc}}$ in the following calculation. The characteristic strength of the magnetic field is $H_0 = \sqrt{\alpha/g_m^{\text{wc}}} \simeq 0.79\sqrt{t}$ (T). We ignore the first-order contribution of the magnetic field to the GL free energy, since it is sizable at a strong magnetic field ~ 1 T, which stabilizes the A_1 phase, while our interest is in weaker magnetic fields on the order of 100 mT. Also, we drop the contribution of the dipole energy which provides negligible contribution to our free energy [21].

B. Bulk energy density

To introduce the basic scales in our problem, let us look at the equilibrium property of the bulk $^3\text{He-B}$ phase without a magnetic field. The B -phase order parameter is written as $A^{(B)} = \Delta_B R(\hat{n}, \phi)$, where Δ_B is the bulk gap amplitude and $R(\hat{n}, \phi)$ is the rotation matrix with an angle ϕ around the axis \hat{n} ; the bulk energy is degenerate with respect to \hat{n} and ϕ . Choosing $\phi = 0$, we have $A^{(B)} = \Delta_B \hat{I}$ with the 3×3 unit matrix \hat{I} . The energy density for the bulk $^3\text{He-B}$ phase is given by

$$f_B^0 = -3\alpha\Delta_B^2 + (9\beta_{12} + 3\beta_{345})\Delta_B^4, \quad (8)$$

where $\beta_{ij} = \beta_i + \beta_j$ and $\beta_{ijk} = \beta_i + \beta_j + \beta_k$. Minimization of this energy density leads to the bulk gap

$$\Delta_B = \sqrt{\frac{\alpha}{\beta'}} \quad (9)$$

and the corresponding energy density

$$f_B^0 = -\frac{3\alpha^2}{2\beta'} \quad (10)$$

with $\beta' = 6\beta_{12} + 2\beta_{345}$.

In this work, a magnetic field $\mathbf{H} = H\mathbf{e}_i$ is applied along the direction which is parallel ($i = z$) and perpendicular ($i = x$) to the vortex axis. The magnitude of H is assumed to be small enough so that the system does not escape from the B phase. To find the suitable range of H , we calculate the bulk free

TABLE II. List of the coefficients for the fitting of the correction of β_j according to the paper by Choi *et al.* [19]. Write ‘‘set II.’’

j	$B_j^{(0)}$	$B_j^{(1)}$	$B_j^{(2)}$	$B_j^{(3)}$	$B_j^{(4)}$	$B_j^{(5)}$	$B_j^{(6)}$	$B_j^{(7)}$	$B_j^{(8)}$	$B_j^{(9)}$
1	0.030472	0.018587	-0.34839	1.0919	-1.66	1.4058	-0.69863	0.2027	-0.031801	0.0020847
2	-0.11014	0.61315	-1.4457	1.8258	-1.5064	0.84442	-0.31656	0.075439	-0.010271	0.00060559
3	0.10094	-1.7982	4.1219	-6.3112	6.4351	-4.2344	1.7664	-0.45099	0.06427	-0.0039131
4	-0.15024	-1.5428	2.8253	-3.82	3.9311	-2.858	1.3449	-0.3822	0.059274	-0.0038433
5	0.16064	0.25229	-0.79652	1.4591	-1.9474	1.655	-0.84977	0.25472	-0.04103	0.0027444

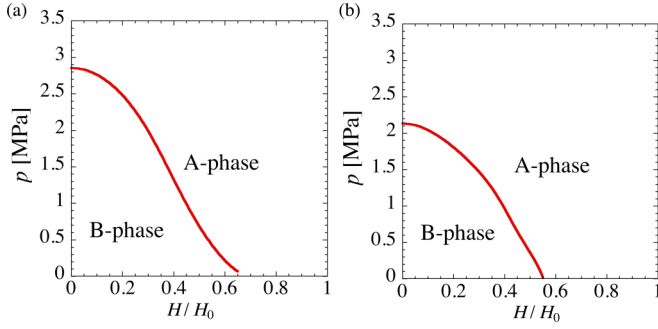


FIG. 2. Bulk phase diagram of superfluid ${}^3\text{He}$ in the p - H plane, calculated from the GL free energy, with set I (a) and set II (b) for strong-coupling corrections.

energy in the magnetic field $\mathbf{H} = H\mathbf{e}_z$. The order parameter of the B phase is modified as

$$A^{(B)} = \begin{pmatrix} \Delta_{\perp} & 0 & 0 \\ 0 & \Delta_{\perp} & 0 \\ 0 & 0 & \Delta_{\parallel} \end{pmatrix}, \quad (11)$$

where

$$\begin{aligned} \Delta_{\perp} &= \Delta_B \sqrt{1 + \frac{\beta_{12} g_m}{\alpha \beta_{345}} H^2}, \\ \Delta_{\parallel} &= \Delta_B \sqrt{1 - \frac{(2\beta_{12} + \beta_{345}) g_m}{\alpha \beta_{345}} H^2}, \end{aligned} \quad (12)$$

and the corresponding energy density is

$$f_B^0 = -\frac{3\alpha^2}{2\beta'} \left[1 - \frac{2g_m H^2}{3\alpha} + \frac{(2\beta_{12} + \beta_{345}) g_m^2 H^4}{3\alpha^2 \beta_{345}} \right]. \quad (13)$$

This energy is compared with that of the bulk A phase characterized by $A^{(A)} = \Delta_A \hat{\mathbf{d}}(\hat{\mathbf{m}} + i\hat{\mathbf{n}})$ with arbitrary unit vectors $\hat{\mathbf{d}}$, $\hat{\mathbf{m}}$, and $\hat{\mathbf{n}}$ such that $\hat{\mathbf{m}} \cdot \hat{\mathbf{n}} = 0$. By choosing $\hat{\mathbf{d}} = \hat{\mathbf{e}}_x$, $\hat{\mathbf{m}} = \hat{\mathbf{e}}_x$, and $\hat{\mathbf{n}} = \hat{\mathbf{e}}_y$, the energy does not depend on the magnetic field; the order parameter and energy density are then given by

$$\Delta_A = \sqrt{\frac{\alpha}{4\beta_{245}}}, \quad f_A^0 = -\frac{\alpha^2}{4\beta_{245}}. \quad (14)$$

By comparing the energies f_B^0 and f_A^0 , we obtain the bulk phase diagram in the p - H plane as shown in Fig. 2. We see qualitatively similar phase diagrams for both data sets of the strong-coupling correction, where the B phase is stable at low pressure and low magnetic field. The area of the stable region of the B phase for set II is smaller than that for set I. Below we confine ourselves within the range $H \lesssim 0.4H_0$ in which the bulk B phase is still the local energy minimum at high pressure.

C. Numerics and boundary condition

We compute the order parameters of vortex states by minimizing the total free energy,

$$F = \int d\mathbf{r} (f_B + f_G + f_M) \quad (15)$$

with the vortex boundary condition. To this end, we evolve the order parameter through the relation

$$\frac{\partial A_{\mu i}}{\partial \tau} = -\frac{\delta F}{\delta A_{\mu i}^*} \quad (16)$$

in two-dimensional Cartesian coordinates, assuming homogeneity along the z direction. Equation (16) is known as the time-dependent GL equation; from a suitable initial state, the order parameter converges to the solution of the energy minimum by time-evolving Eq. (16). Here, τ is called the imaginary time. Axisymmetry cannot be assumed *a priori* because the d vortex breaks it spontaneously.

We use the temperature-dependent coherence length $\xi(t) = \sqrt{K/\alpha(t)}$, Δ_B in Eq. (9), and $|f_B^0|$ in Eq. (10) to scale the length, the order parameter, and the energy density, respectively. Then, the dimensionless order parameter and the free energy is written as $\tilde{A}_{\mu i} = A_{\mu i}/\sqrt{\alpha(t)/\beta'}$ and

$$\tilde{F} \equiv \frac{F}{|f_B^0| \xi^2(t)} = \int d\tilde{\mathbf{r}} \frac{2}{3} (\tilde{f}_B + \tilde{f}_G + \tilde{f}_M), \quad (17)$$

respectively, where tildes denote the dimensionless variables. Also, by scaling the magnetic field as $H = H_0 \tilde{H}$, the energy density on the right hand side of Eq. (17) can be written by just replacing the coefficients in Eqs. (2), (4), and (6) as

$$\begin{aligned} \alpha &\rightarrow 1, & \beta_j &\rightarrow \frac{\beta_j}{\beta'} = \frac{\beta_j^{\text{wc}} + \Delta\beta_j}{\beta'}, \\ K &\rightarrow 1, & g_m &\rightarrow \frac{g_m(p)}{g_m(0)} \approx 1. \end{aligned} \quad (18)$$

Then, all physical quantities become dimensionless.

We take a system size for numerical simulations as $\tilde{x}, \tilde{y} \in [-50, 50]$ with a 500×500 numerical grid. Although we solve Eq. (16) in the xy coordinates, we impose the Dirichlet boundary condition for the vortex structure on the cylinder with the radius $\tilde{R} = 50$. The boundary condition is taken as $\lim_{\tilde{r} \rightarrow \tilde{R}} \tilde{A}_{\mu i}(\tilde{r}, \theta) = \hat{\mathbf{l}} e^{i\theta}$, where (\tilde{r}, θ) is the dimensionless polar coordinate. This means that far from the vortex core at the center, the order parameter approaches the bulk value with unit phase winding. However, as shown by Hasegawa [22], the asymptotic form of the off-diagonal components of $\tilde{A}_{\mu i}$, some of which occupy the vortex core, decays slowly as $\sim r^{-1}$, and we have to take a large system size to ensure the validity of this boundary condition. We confirm that $\tilde{R} = 50$ is large enough to ignore the finite size effect on the vortex energy. Furthermore we avoid the unfavorable boundary contribution to the vortex energy by integrating Eq. (17) within the region $\tilde{R} \leq 40$ when calculating the total energy.

D. Vortex state without a magnetic field

Here, we briefly review the vortex state without a magnetic field. Typically, there are three types of solutions, known as the o vortex, the v vortex, and the d vortex. Thuneberg analyzed these vortex states and calculated their energies within the GL theory with β values obtained from set I [10,11]. Here, we calculate them not only with set I but also with set II, obtaining qualitatively similar results for both data sets; the typical spatial profiles of the order parameters for set II are

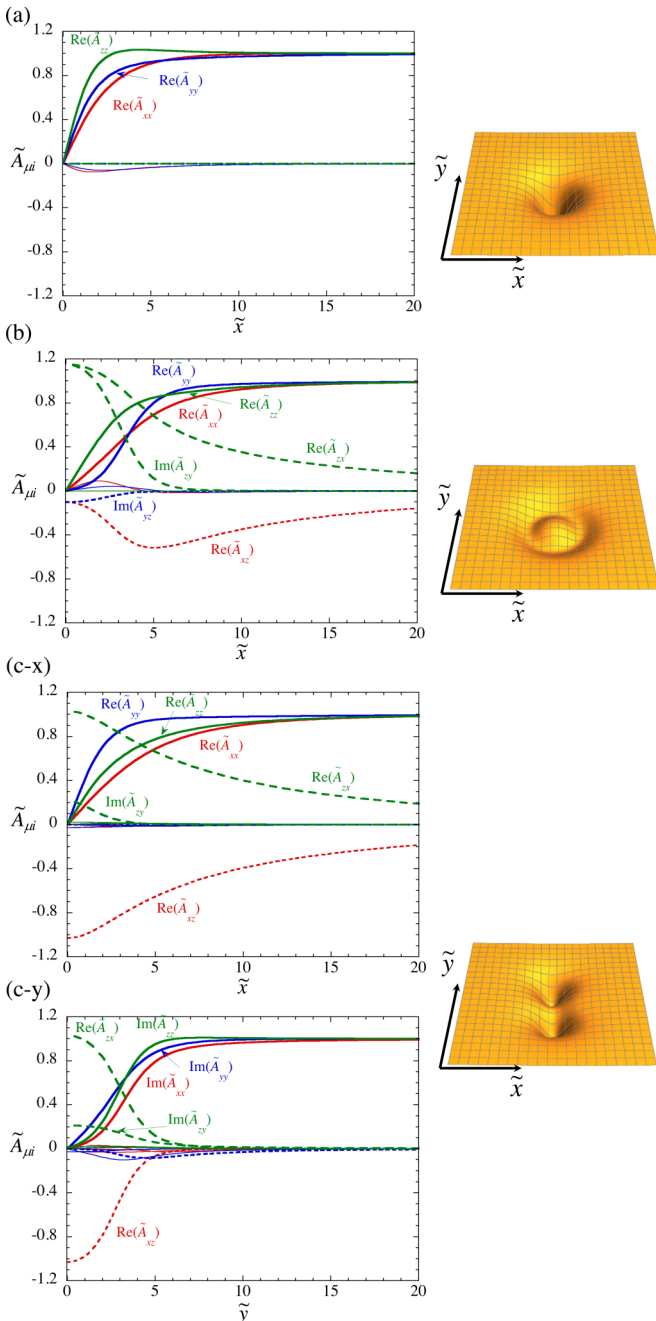


FIG. 3. (Left) Typical radial profiles of the order parameters for (a) the *o* vortex, (b) the *v* vortex, and (c) the *d* vortex. Here the strong-coupling correction set II is employed and the pressure is set to 3.0 MPa. Because the *d* vortex is not axisymmetric, we show the profiles along the \tilde{x} and \tilde{y} axes as (c-x) and (c-y), respectively. Diagonal components of $(\tilde{A}_{\mu i})$ are shown in solid curves, while off-diagonal ones in dashed curves. (Right) Corresponding 2D profiles of the pair density $\sum_{\mu,i} |\tilde{A}_{\mu i}|^2$.

shown in Fig. 3 and the vortex energy as a function of p is shown in Fig. 4.

The *o* vortex has an axisymmetric structure and the core is not filled with any superfluid components. The *v* vortex is also axisymmetric but has a core filled mainly with the *A*-phase components $\text{Re}(\tilde{A}_{zx})$ and $\text{Im}(\tilde{A}_{zy})$, whose amplitudes take the

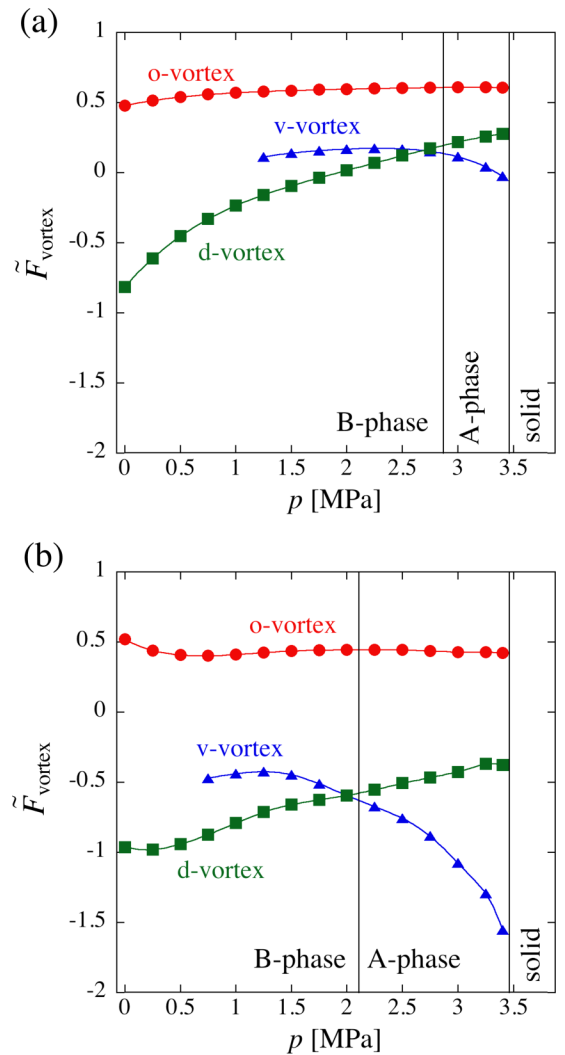


FIG. 4. Free energies of the three vortex states without a magnetic field as functions of the pressure p for set I (a) and set II (b). The energies of the *o*, *v*, and *d* vortices are shown by curves with red circles, blue triangles, and green squares, respectively. The bulk *A*-*B* phase boundary is taken from Fig. 2.

same value at the origin. There are also minor components $\text{Re}(\tilde{A}_{xz})$ and $\text{Im}(\tilde{A}_{yz})$ filling the vortex core, which are known as the β phase. The fraction of the *A*-phase component increases as the pressure increases.

The *d* vortex is a nonaxisymmetric vortex as seen in Figs. 3(c-x) and (c-y), where the profiles are different along the \tilde{x} direction and \tilde{y} direction. The core components are $\text{Re}(\tilde{A}_{zx})$ and $\text{Re}(\tilde{A}_{xz})$, corresponding to the planar phase characterized by $\tilde{A} = \tilde{\Delta}_p R(\hat{n}, \phi)(I - \hat{w}\hat{w})$ with $\hat{n} = \hat{w} = \mathbf{e}_y$ and $\phi = \pi/2$ [11]. In this case, there appear double vortex cores along the \tilde{y} direction. The vortex energy is calculated by subtracting \tilde{F}_{bulk} and \tilde{F}_{hyd} from the total free energy \tilde{F} in Eq. (17) as

$$\tilde{F}_{\text{vortex}} = \tilde{F} - \tilde{F}_{\text{bulk}} - \tilde{F}_{\text{hyd}}. \quad (19)$$

Here, $\tilde{F}_{\text{bulk}} = 1 \times S$ is the bulk free energy with the system area S and $F_{\text{hyd}} = \int d\mathbf{r} \sum_k \rho_k v_k^2/2$ is a hydrodynamic kinetic energy caused by vortex flow. The energy F_{hyd} can be

calculated by combining the relation $j_k = \rho_k v_{sk}$ ($k = x, y, z$) for the superfluid density ρ_k and the current density

$$j_k = \frac{4m_3K}{\hbar} \text{Im}[A_{\mu k}^* \partial_j A_{\mu j} + A_{\mu j}^* \partial_k A_{\mu j} + A_{\mu j}^* \partial_j A_{\mu k}]. \quad (20)$$

The dimensionless form of F_{hyd} is $\tilde{F}_{\text{hyd}} = (20\pi/3) \ln[R/\xi(t)]$ with the radius R of the cylinder, where the lower bound of the integral has been taken as $\xi(t)$.

For set I, we reproduce the results of Thuneberg [10,11] as seen in Fig. 4(a) and confirm the validity of our calculation. The o vortex is always the highest energy configuration. For low pressures, the d vortex is the most stable vortex state, while the v vortex is most stable above $p \simeq 2.7$ MPa. In our two-dimensional calculation without axisymmetry, the v vortex is energetically unstable for low pressures below 1.25 MPa and it decays to the d vortex. Similar behavior has also been mentioned by Thuneberg [11].

Figure 4(b) shows the energy of the vortex states for set II. Although the result qualitatively agrees with that in Fig. 4(a), we confirm quantitative differences. Especially, the critical pressure for the transition between the v vortex and the d vortex is remarkably reduced to ≈ 2.0 MPa, compared to that of ≈ 2.7 MPa seen in Fig. 4(a). Thus the results for set II explains the experimental observation of the vortex-core transition [3,10] for $T \simeq T_c$ more accurately than those for set I. Note that the transition pressure of the v and the d vortices is close to the boundary of the bulk AB transition for both set I and set II.

III. VORTEX STATE IN MAGNETIC FIELD

In this section, we consider the effect of a magnetic field \mathbf{H} on the vortex states. We address two situations: one with the parallel magnetic field $\mathbf{H} = H\mathbf{e}_z$, and the other with the perpendicular magnetic field $\mathbf{H} = H\mathbf{e}_x$.

A. Parallel magnetic field

Here we consider the vortices under a magnetic field along the z axis. The effect of the axial magnetic field can be understood by examining the free energy functional. The quadratic magnetic-field term Eq. (6) for $\mathbf{H} = H\mathbf{e}_z$ is written as $\tilde{f}_M = \tilde{H}^2 \sum_i |\tilde{A}_{zi}|^2$. Thus the population of the core components whose spin is along the z direction in the v and d vortices should be suppressed to reduce the energy cost. Then, it is not trivial to tell which vortex state has the lowest energy.

To obtain the vortex solution under the magnetic field, we should fix the boundary condition, i.e., the proper choice of $R(\hat{\mathbf{n}}, \phi)$ at the boundary. In the bulk region, by taking account of the quadratic magnetic energy and the dipole-dipole energy, the $\hat{\mathbf{n}}$ should be parallel to \mathbf{H} , since the combination of these energies gives an energy contribution $\propto -(\hat{\mathbf{n}} \cdot \mathbf{H})^2$ [11]. Also, the dipole-dipole energy fixes $\phi = \arccos(-1/4)$. Since the vortices are along the z axis in our problem, the vortex structures including the core components as well as the vortex energies are not affected by the rotation $R(\hat{\mathbf{z}}, \phi)$ of the order parameter at the boundary. Thus we set the bulk amplitude with $\phi = 0$ as the Dirichlet boundary condition at $r = R$, and

write the order parameter at the boundary as

$$\tilde{A}^{(B)} = \begin{pmatrix} \tilde{\Delta}_\perp & 0 & 0 \\ 0 & \tilde{\Delta}_\perp & 0 \\ 0 & 0 & \tilde{\Delta}_\parallel \end{pmatrix} e^{i\theta}, \quad (21)$$

where $\tilde{\Delta}_\perp$ and $\tilde{\Delta}_\parallel$ are given by Eqs. (12). The vortex energy Eq. (19) is calculated in a similar way as that described in Sec. IID. Here, \tilde{F}_{bulk} is evaluated from the spatial integral of Eq. (13) and $\tilde{F}_{\text{hyd}} = (4\pi/3)(4\tilde{\Delta}_\perp^2 + \tilde{\Delta}_\parallel^2) \ln(R/\xi(t))$.

Figure 5 shows the vortex free energy $\tilde{F}_{\text{vortex}}$ of the three vortex states as a function of pressure for several \tilde{H} . The main feature of Fig. 5 for both sets of the strong-coupling correction is that the d vortex is the most preferable structure under the magnetic field. The v vortex has a local minimum only in the high-pressure region, which shrinks and eventually disappears as the magnetic field strength increases; the initial v vortex relaxes to the d vortex through the evolution of Eq. (16) when the v vortex is unstable. The o vortex is always the highest energy state, being metastable in all situations. Although we solved Eq. (16) with other initial configurations, the final states of the imaginary time evolution are always one of the three vortices.

Let us see the details of the magnetic field dependence of the v - and the d -vortices in the high pressure region. The free energy of the v vortex increases with H , while that of the d vortex decreases, as shown in Fig. 5(d). This inverts the energetic stability of the two vortex states at a critical magnetic field. Figure 6 shows the phase diagram of the stability of the v and d vortices. In addition to the above critical magnetic field, there is another one which gives metastability of the v vortex. These critical magnetic fields monotonically increase with the pressure.

The p -dependence of the critical magnetic field can be qualitatively understood by comparing the free energy of the bulk A phase and that of the planar phase. The vortex core is filled with these phases. For the A phase in the core of the v vortex, described by $\text{Re}(\tilde{A}_{zx}) = \text{Im}(\tilde{A}_{zy}) \equiv \tilde{\Delta}_{A1}$, the bulk amplitude and the minimized energy are given by

$$\begin{aligned} \tilde{\Delta}_{A1}^2 &= \frac{\beta'(1 - \tilde{H}^2)}{4\beta_{245}}, \\ \tilde{f}_A^H &= -\frac{\beta'(1 - \tilde{H}^2)^2}{6\beta_{245}}. \end{aligned} \quad (22)$$

Here, we ignore the minor β -phase components for simplicity. For the planar phase in the d vortex, we take the components $\text{Re}(\tilde{A}_{zx}) \equiv \tilde{\Delta}_{p1}$ and $\text{Re}(\tilde{A}_{xz}) \equiv -\tilde{\Delta}_{p2}$, and the bulk amplitude and the minimized energy are

$$\begin{aligned} \tilde{\Delta}_{p1}^2 &= \frac{\beta'[\beta_{345} - \tilde{H}^2(\beta_{12} + \beta_{345})]}{2\beta_{345}(2\beta_{12} + \beta_{345})}, \\ \tilde{\Delta}_{p2}^2 &= \frac{\beta'(\beta_{12}\tilde{H}^2 + \beta_{345})}{2\beta_{345}(2\beta_{12} + \beta_{345})}, \\ \tilde{f}_p^H &= -\frac{\beta'[\beta_{345}(2 - 2\tilde{H}^2 + \tilde{H}^4) + \beta_{12}\tilde{H}^4]}{6\beta_{345}(2\beta_{12} + \beta_{345})}. \end{aligned} \quad (23)$$

For a given pressure, \tilde{f}_p^H becomes lower than \tilde{f}_A^H at a certain magnetic field, which is shown by a thin dashed curve in the phase diagram of Fig. 6. The dashed curve has a similar

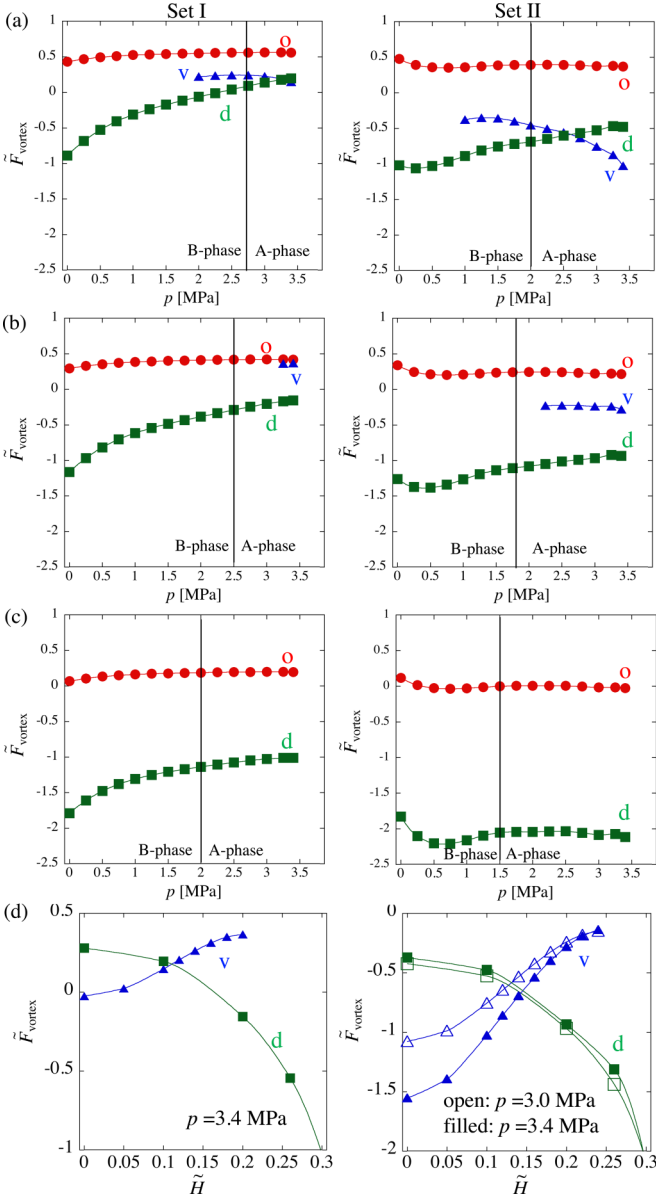


FIG. 5. Free energies of the three vortex states as functions of pressure p for set I (left panels) and set II (right panels). The magnitude of the magnetic field is (a) $\tilde{H} = 0.1$, (b) 0.2, and (c) 0.3. The energies of the o , v , and d vortices are shown by curves with red circles, blue triangles, and green squares, respectively. The bulk A - B phase boundary is taken from Fig. 2. The figures (d) show the free energies of the v and d vortices as functions of \tilde{H} in the high-pressure region; we show the plots with $p = 3.0$ MPa for set I and with $p = 3.0$ and 3.4 MPa for set II.

pressure dependence as the critical magnetic fields described above. Thus we expect that the occupation of the planar-phase component is energetically more favorable than the A -phase component in the vortex core in the presence of a parallel magnetic field.

B. Perpendicular magnetic field

We turn to the analysis on the vortices in the perpendicular magnetic field. Let us consider $\mathbf{H} = H\mathbf{e}_x$. Then, the magnetic

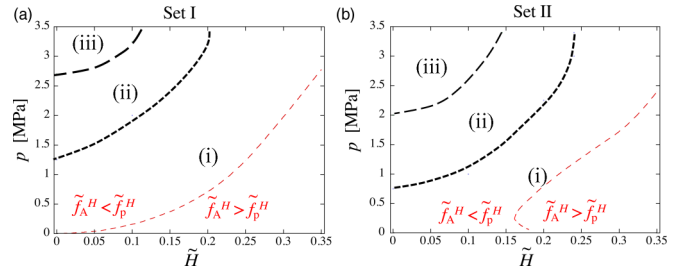


FIG. 6. p - H phase diagram of the stable v - and d -vortex states for (a) set I and (b) set II of the strong-coupling corrections. The regions of the phase diagram are separated into (i) v vortex is unstable and d vortex is stable, (ii) v vortex is metastable and d vortex is stable, (iii) v vortex is stable and d vortex is metastable. The (red) thin-dashed curve represents the phase boundary of the bulk A phase and bulk planar phase, which is obtained by comparing the free energies in Eqs. (22) and (23).

free energy written as $\tilde{F}_M = \tilde{H}^2 \sum |\tilde{A}_{xi}|^2$ leads to suppression of the components $|\tilde{A}_{xi}|$. Here, we should take the boundary condition

$$R(\hat{x}, \phi) \tilde{A}^{(B)} e^{i\theta} = \begin{pmatrix} \tilde{\Delta}_{\parallel} & 0 & 0 \\ 0 & \tilde{\Delta}_{\perp} \cos \phi & -\tilde{\Delta}_{\perp} \sin \phi \\ 0 & \tilde{\Delta}_{\perp} \sin \phi & \tilde{\Delta}_{\perp} \cos \phi \end{pmatrix} e^{i\theta} \quad (24)$$

at the boundary $r = R$, where $\tilde{A}^{(B)} = \text{diag}(\tilde{\Delta}_{\parallel}, \tilde{\Delta}_{\perp}, \tilde{\Delta}_{\perp})$ with Eq. (12). Then, it is not trivial how the rotation angle ϕ at the boundary affects the vortex structures, because the components \tilde{A}_{yz} and \tilde{A}_{zy} appearing in the vortex cores are influenced by the choice of the angle ϕ . More precisely, when $\phi \neq 0$, not only the components \tilde{A}_{yy} and \tilde{A}_{zz} but also \tilde{A}_{yz} and \tilde{A}_{zy} should have zeros around the origin for the nonzero winding number. We confirm that the character of all vortices is independent of ϕ as shown later; the internal structure of the vortex core adjusts to the given boundary condition without changing the free energy.

Here, we analyze the vortex structure by employing the boundary condition (24) with $\phi = 0$. There are two main effects of $\mathbf{H} = H\mathbf{e}_x$ on the core structures. One is the stabilization of the v vortex. The other is to lock the orientation of the double cores of the d vortex along the x or y direction; we refer to the former and the latter as d_x vortex and d_y vortex, respectively. Figure 7 shows the vortex energy $\tilde{F}_{\text{vortex}}$ as a function of the pressure, while Fig. 8 depicts a magnified view of Fig. 7 in the vicinity of the transition point by taking only the energies of the v , d_x , and d_y vortices. For $\tilde{H} = 0.1$, the qualitative stability properties of the vortex states are not changed from those for $\tilde{H} = 0$. However, the energy of the d_x vortex is slightly lower than that of the d_y vortex. With increasing the magnetic field to $\tilde{H} = 0.2$, the stability region of the v vortex extends to the lower pressure region. Also, the d_y vortex becomes unstable in the high pressure region, decaying into the symmetric v vortex. Above $\tilde{H} = 0.2$, the d_y vortex continuously transforms to the v vortex as p increases. No hysteresis is observed in this transition. The d_x vortex is stable in the low-pressure region and survives as a metastable state for higher pressures. With increasing to $\tilde{H} = 0.3$, although the d_x vortex exists as a metastable state in the low pressure region, the v vortex becomes the most stable

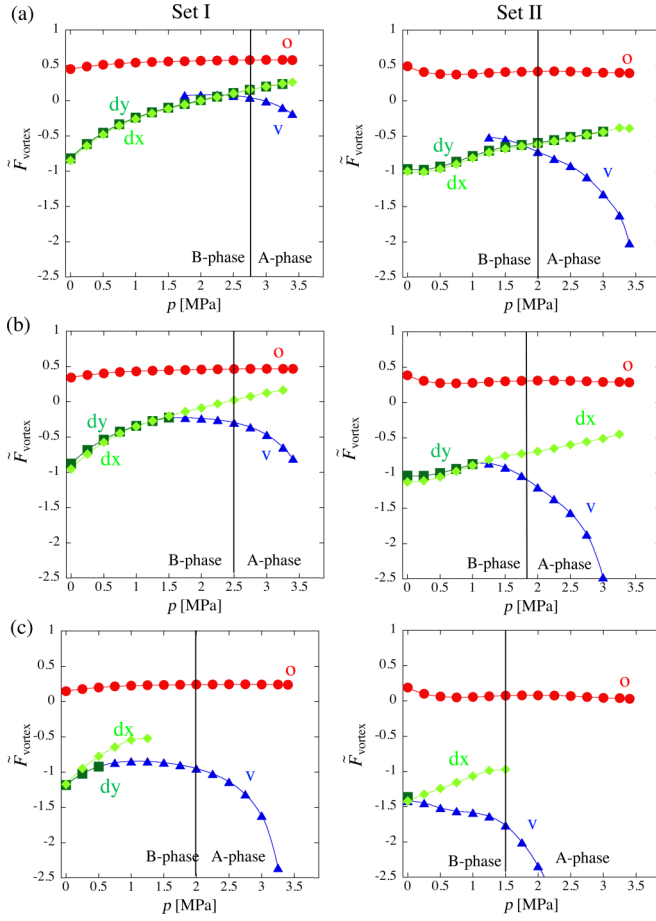


FIG. 7. Free energies of the vortex states in the presence of a magnetic field perpendicular to the vortex axis as a function of the pressure p for set I (left panels) and set II (right panels). The magnitude of the magnetic field is (a) $\tilde{H} = 0.1$, (b) 0.2, and (c) 0.3. The energies of the o , v , d_y , and d_x vortices are shown by curves with red circles, blue triangles, green squares, and yellow green diamonds, respectively. The bulk A - B phase boundary is taken from Fig. 2.

state. For higher pressures (above 3.25 MPa for set I and 2.25 MPa for set II), the vortex state is unstable to become the bulk A phase without vorticity. Similarly to the results in Sec. III A, the o vortex is always metastable.

In order to understand the above properties, it is useful to consider the bulk free energy of the core components. The order parameter of the planar phase in the d vortex and the rotation angle φ of the orientation of the splitting double core are related with

$$\tilde{A}^{\text{pl}} = \begin{pmatrix} 0 & 0 & -\tilde{\Delta}_{p2}a(\varphi) \\ 0 & 0 & -\tilde{\Delta}_{p2}b(\varphi) \\ \tilde{\Delta}_{p1}a(\varphi) & \tilde{\Delta}_{p1}b(\varphi) & 0 \end{pmatrix} \quad (25)$$

with $a(\varphi) = \cos^2 \varphi - i \sin \varphi \cos \varphi$ and $b(\varphi) = -\sin \varphi \cos \varphi + i \sin^2 \varphi$. Here, $\varphi = 0$ and $\pi/2$ correspond to the d_y and d_x vortices, respectively, where the profiles of the order parameters are shown in Fig. 3(c) for the d_y vortex and Fig. 9 for the d_x vortex. Then, the bulk free energy f_B is independent of φ but the quadratic magnetic free energy for $\mathbf{H} = H\mathbf{e}_x$ is written as $\tilde{f}_M = \alpha \tilde{\Delta}_{p2}^2 \tilde{H}^2 \cos^2 \varphi$. In the bulk, the magnetic free energy is minimized for $\varphi = \pi/2$. This feature is consistent with our

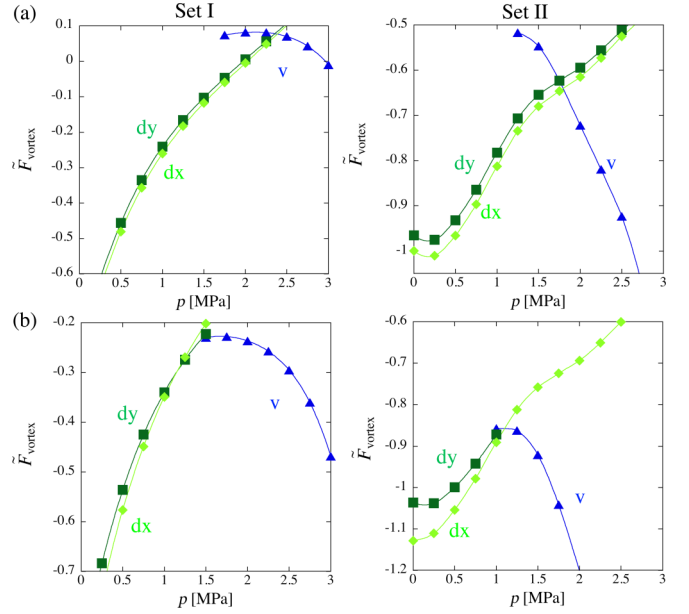


FIG. 8. Free energies of the v , d_y , and d_x vortex states in the presence of a magnetic field perpendicular to the vortex axis as a function of the pressure p for set I (left panels) and set II (right panels) for (a) $\tilde{H} = 0.1$ and (b) 0.2. The figures are the enlarged view of Figs. 7(a) and 7(b) in the vicinity of the transition pressure.

observation in Fig. 8. We confirm that, through the imaginary time evolution from the initial states with $0 < \varphi < \pi/2$, the solutions always converge to those with $\varphi = 0$ or $\varphi = \pi/2$. This implies that there is an energy barrier between d_x and d_y vortices and the barrier originates from \tilde{f}_G .

The continuous structural change between the d_y vortex and the v vortex can be analyzed by carefully examining

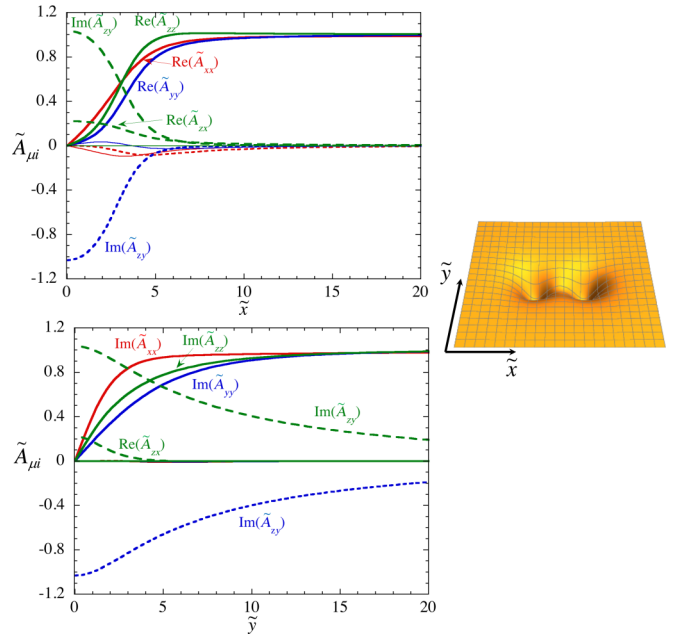


FIG. 9. Typical radial profiles of the order parameter (left) and the 2D profile of the pair density $\sum_{\mu,i} |\tilde{A}_{\mu i}|^2$ (right) of the d_x vortex for $p = 3.0$ MPa and $\tilde{H} = 0.2$.

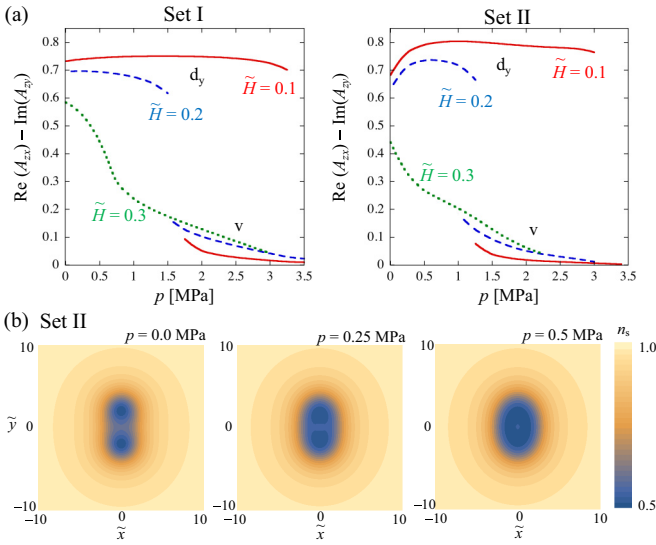


FIG. 10. Transition from the d_y vortex to the v vortex as p is varied. In (a), the difference $\text{Re}(\tilde{A}_{zx}) - \text{Im}(\tilde{A}_{zy})$ at the origin $x = y = 0$ is shown as a function of p for $\tilde{H} = 0.1, 0.2, 0.3$. The left and the right panels correspond to set I and set II, respectively. The panels in (b) show the contour plots of the pair density $\sum_{\mu,i} |\tilde{A}_{\mu,i}|^2$ for $\tilde{H} = 0.3$ and $p = 0, 0.25, \text{ and } 0.5$ MPa from left to right with set II.

the core components. For the boundary condition (24) with $\phi = 0$, the distribution of $\text{Re}(\tilde{A}_{xz})$ and $\text{Re}(\tilde{A}_{zx})$ in the v and d_y vortices are similar to each other, which allows the continuous transformation between the two structures. The angle φ of the double core has to be rotated by $\pi/2$ for the d_x vortex to have similar distributions of $\text{Re}(\tilde{A}_{xz})$ and $\text{Re}(\tilde{A}_{zx})$ with those in the v vortex. This is prohibited by the energy barrier stated above and ensures the presence of the metastable d_x vortex in the high pressure region as seen in Figs. 7 and 8. The change from the d_y vortex to the v vortex can be understood

by examining the core components at the origin. Figure 10(a) shows the difference $\text{Re}(\tilde{A}_{zx}) - \text{Im}(\tilde{A}_{zy})$ at the origin as a function of the pressure; the finite difference implies the d_y vortex with the planar phase core, while the zero difference signifies the v vortex with the A -phase core. For $\tilde{H} = 0.1$, there is a hysteresis of the transition between the two vortex states. As \tilde{H} is increased to 0.2, there appears a jump of the difference without hysteresis. For $\tilde{H} = 0.3$, the difference monotonically decreases as p increases, where the continuous change from the d_y vortex to the v vortex takes place as p increases, as shown in Fig. 10(b). We should note that for $H \neq 0$ the v vortex has the finite difference $\text{Re}(\tilde{A}_{zx}) - \text{Im}(\tilde{A}_{zy})$ in the core components, which should be referred to as the *nonaxisymmetric v vortex*.

We checked that the vortex energies are independent of a change of the boundary condition associated with the angle ϕ of Eq. (24). In Fig. 11, we show the profile of the order parameters of v , d_y , and d_x vortices for $\phi = \pi/4$. Then, the components \tilde{A}_{yy} , \tilde{A}_{yz} , \tilde{A}_{zy} , and \tilde{A}_{zz} should have zeros around the origin because of the boundary condition with a phase winding, despite the fact that \tilde{A}_{yz} and \tilde{A}_{zy} should occupy the vortex core in each vortex state. Figure 11 shows that zeros of the order parameter appear at the positions displaced from the origin along the y direction. We find numerically that the total energy as well as the total pair density $\sum_{\mu,i} |\tilde{A}_{\mu,i}|^2$ are invariant with respect to ϕ .

Finally, our results are summarized in the p - H phase diagram of Fig. 12. As an overall feature, with increasing perpendicular magnetic field \tilde{H} , the stable region of the d vortex gradually shrinks, while that of the v vortex gradually expands.

IV. CONCLUSION

In this paper, we study the vortex states in superfluid $^3\text{He-B}$ phase under magnetic fields parallel and perpendicular to the

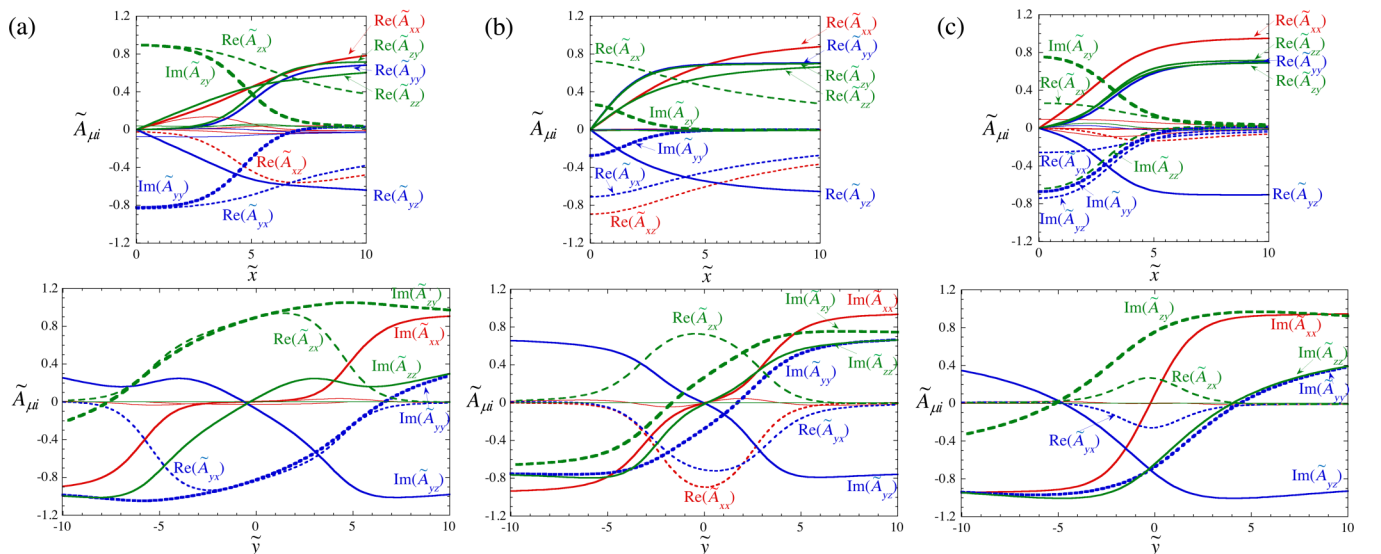


FIG. 11. The cross section of the order parameter A along the x (top) and the y (bottom) axes for (a) the v vortex ($p = 3.0$ MPa), (b) the d_y vortex ($p = 0.0$ MPa), and (c) the d_x vortex ($p = 0.0$ MPa) for $\tilde{H} = 0.2$, obtained with the boundary condition Eq. (24) with $\phi = \pi/4$. In all cases, the distributions of the core components along the x axis have inversion symmetry at the origin, but those along the y direction do not.

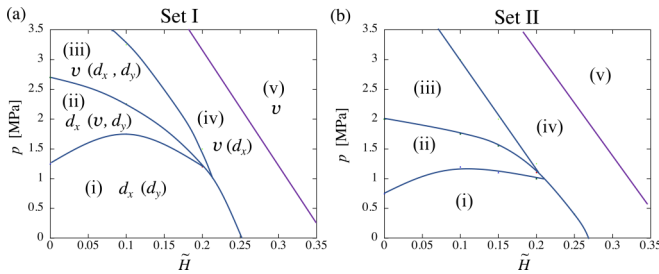


FIG. 12. p - H phase diagram of the stable v - and d vortex states for (a) set I and (b) set II of the strong-coupling corrections. The p - H plane is divided into (i) the d_x vortex is stable and the d_y vortex is metastable, (ii) the v vortex is metastable, the d_x vortex is stable, and the d_y vortex is metastable, (iii) the v vortex is stable and the d_x and d_y vortices are metastable, (iv) the v vortex is stable and the d_x vortex is metastable, and (v) the v vortex is stable.

vortex axis within the GL theory. We calculate the free energy of the o , v , and d vortices with two different sets of the strong-coupling corrections, set I and set II, finding that the results for set II reproduce quantitatively the experimental data at zero magnetic fields. Under a magnetic field along the z axis (the axis of the vortex), the v vortex, which is stable at high pressure and zero magnetic field, becomes unstable and decays to the d vortex. On the other hand, if the magnetic field is applied along the x -axis, perpendicular to the axis of the vortex, the v vortex is the most stable state at high magnetic field. In the latter case, the anisotropic features of the vortex structure are more remarkable, as the d_x and d_y vortices exist as distinct energy minima. We estimate that these transitions take place at $H \sim 0.2H_0 \sim 50$ mT, when $T = 0.9T_c$, which is observable in a suitable experimental setup [3,9,13].

The dependence of the vortex structure on the magnetic field can be understood qualitatively by the energetic argument of the core-occupying components of the order parameter. A magnetic field applied to bulk superfluid ^3He stabilizes the A phase more than the B phase in general.

The d vortex tends to be stabilized in the presence of a magnetic field along the z axis. Recall that the core of the v vortex is filled with the A phase with nonvanishing order parameter components A_{zi} ($i = x, y$), which are suppressed by the magnetic field along the z axis. This makes the v vortex energetically unfavorable compared to the d vortex. This is rather counterintuitive since a magnetic field stabilizes the bulk A phase. A magnetic field along the x axis suppresses the order parameter components A_{xi} ($i = x, y, z$). The core of the v vortex is filled with the components A_{zx} and A_{zy} , while that of the d_x vortex, the stable d vortex in this case, is filled with the planar phase with dominant components $\text{Im}A_{yz}$ and $\text{Im}A_{zy}$. These core components are not suppressed by the perpendicular magnetic field. However, the v vortex is more stable than the d_x vortex when the perpendicular magnetic field is strong enough since a magnetic field energetically favors the A phase compared to the planar phase for bulk superfluid ^3He . It is noticeable that these properties are qualitatively consistent with the magnetic susceptibilities calculated by Thuneberg in Ref. [11], where the d vortex has higher susceptibility in the z direction than the v vortex and vice versa in the x (or equivalently y) direction. Also, the d vortex has the higher susceptibility in the orientation of the double cores. As a further study, it would be interesting to see the effect of a magnetic field applied at intermediate angles to the vortex axis.

ACKNOWLEDGMENTS

We would like to thank Erkki Thuneberg and Matti Krusius for their interest in this work. They also read the manuscript carefully and gave useful comments. The work of K.K. is partly supported by KAKENHI from the Japan Society for the Promotion of Science (JSPS) Grant-in-Aid for Scientific Research (KAKENHI Grant No. 18K03472). The work of M.N. is partly supported by KAKENHI from the JSPS Grant-in-Aid for Scientific Research (KAKENHI Grant No. 17K05554).

-
- [1] D. Vollhardt and P. Wölfle, *The Superfluid phase of Helium 3* (Taylor and Francis, London, 1990).
- [2] M. M. Salomaa and G. E. Volovik, Quantized vortices in superfluid ^3He , *Rev. Mod. Phys.* **59**, 533 (1987).
- [3] M. Krusius, The vortices of superfluid ^3He , *J. Low Temp. Phys.* **91**, 233 (1993).
- [4] M. M. Salomaa and G. E. Volovik, Vortices with Ferromagnetic Superfluid Core in $^3\text{He-B}$, *Phys. Rev. Lett.* **51**, 2040 (1983).
- [5] M. M. Salomaa and G. E. Volovik, Symmetry and structure of quantized vortices in superfluid $^3\text{He-B}$, *Phys. Rev. B* **31**, 203 (1985).
- [6] T. Ohmi, T. Tsuneto, and T. Fujita, Core structure of vortex line in $^3\text{He-B}$, *Prog. Theor. Phys.* **70**, 647 (1983).
- [7] S. Theodorakis and A. Fetter, Vortices and NMR in rotating $^3\text{He-B}$, *J. Low Temp. Phys.* **52**, 559 (1983).
- [8] T. Passvogel, L. Tewordt, and N. Schopohl, Stability, orientational effects, and temperature dependence of nonunitary vortex structures in superfluid ^3He , *J. Low Temp. Phys.* **56**, 383 (1984).
- [9] P. J. Hakonen, M. Krusius, M. M. Salomaa, J. T. Simola, Y. M. Bunkov, V. P. Mineev, and G. E. Volovik, Magnetic Vortices in Rotating Superfluid $^3\text{He-B}$, *Phys. Rev. Lett.* **51**, 1362 (1983).
- [10] E. V. Thuneberg, Identification of Vortices in Superfluid $^3\text{He-B}$, *Phys. Rev. Lett.* **56**, 359 (1986).
- [11] E. V. Thuneberg, Ginzburg-Landau theory of vortices in superfluid $^3\text{He-B}$, *Phys. Rev. B* **36**, 3583 (1987).
- [12] M. M. Salomaa and G. E. Volovik, Vortices with Spontaneously Broken Axisymmetry in $^3\text{He-B}$, *Phys. Rev. Lett.* **56**, 363 (1986).
- [13] Y. Kondo, J. S. Korhonen, M. Krusius, V. V. Dmitriev, Y. M. Mukharsky, E. B. Sonin, and G. E. Volovik, Direct Observation of the Nonaxisymmetric Vortex in Superfluid $^3\text{He-B}$, *Phys. Rev. Lett.* **67**, 81 (1991).

- [14] M. Fogelström and J. Kurkijärvi, Quasiclassical theory of vortices in $^3\text{He-B}$, *J. Low Temp. Phys.* **98**, 195 (1995); On the local stability of the quadrupole vortex in superfluid $^3\text{He-B}$, *ibid.* **116**, 1 (1999).
- [15] Y. Tsutsumi, T. Kawakami, K. Shiozaki, M. Sato, and K. Machida, Symmetry-protected vortex bound state in superfluid $^3\text{He-B}$ phase, *Phys. Rev. B* **91**, 144504 (2015).
- [16] M. A. Silaev, E. V. Thuneberg, and M. Fogelström, Lifshitz Transition in the Double-Core Vortex in $^3\text{He-B}$, *Phys. Rev. Lett.* **115**, 235301 (2015).
- [17] J. A. Sauls and J. W. Serene, Comment on “Symmetry and structure of quantized vortices in superfluid $^3\text{He-B}$ ”, *Phys. Rev. B* **32**, 4782 (1985).
- [18] J. A. Sauls and J. W. Serene, Potential-scattering models for the quasiparticle interactions in liquid ^3He , *Phys. Rev. B* **24**, 183 (1981).
- [19] H. Choi, J. P. Davis, J. Pollanen, T. M. Haard, and W. P. Halperin, Strong coupling corrections to the Ginzburg-Landau theory of superfluid ^3He , *Phys. Rev. B* **75**, 174503 (2007); **87**, 019904(E) (2013).
- [20] J. J. Wiman and J. A. Sauls, Strong-coupling and the stripe phase of ^3He , *J. Low Temp. Phys.* **184**, 1054 (2016).
- [21] E. V. Thuneberg, Hydrostatic theory of superfluid $^3\text{He-B}$, *J. Low Temp. Phys.* **122**, 657 (2001).
- [22] Y. Hasegawa, On vortex in superfluid $^3\text{He-B}$, *Prog. Theor. Phys.* **73**, 1258 (1985).